Macromolecules

Article

pubs.acs.org/Macromolecules

Star Diblock Copolymer Concentration Dictates the Degree of Dispersion of Carbon Black Particles in Nonpolar Media: Bridging Flocculation versus Steric Stabilization

David J. Growney,[†] Oleksandr O. Mykhaylyk,*[,†] Thibault Derouineau,[†] Lee A. Fielding,[†] Andrew J. Smith,[‡] Najib Aragrag,[§] Gordon D. Lamb,[§] and Steven P. Armes*[,†]

[†]Department of Chemistry, University of Sheffield, Brook Hill, Sheffield, South Yorkshire S3 7HF, U.K.

[‡]Diamond Light Source Ltd., Diamond House, Harwell Science and Innovation Campus, Didcot, Oxfordshire OX11 0DE, U.K.

[§]BP Formulated Products Technology, Technology Centre, Whitchurch Hill, Pangbourne RG8 7QR, U.K.

Supporting Information

ABSTRACT: The solution behavior of a polystyrene–hydrogenated polyisoprene star diblock copolymer (M_n ~ 384 K; 6 mol % polystyrene) is examined in nonpolar media. Variable temperature ^{1}H NMR studies using deuterated *n*-dodecane confirm that the outer polystyrene blocks are only partially solvated in *n*-dodecane at 25 °C: the apparent polystyrene content of 3.2 ± 0.2 mol % remains essentially constant on heating up to 100 °C. Physical adsorption of this star diblock copolymer onto carbon black particles is examined, with particular attention being paid to the effect of copolymer concentration on colloidal stability. An isotherm is constructed for copolymer adsorption onto carbon black from *n*-dodecane at 20 °C using a supernatant depletion assay based on UV spectroscopy analysis of the aromatic chromophore in the polystyrene block. Langmuir-type adsorption is observed with a maximum adsorbed amount, Γ, of ~2.2 ± 0.1 mg m^{-2}. In addition, thermogravimetric analysis is used to directly determine the amount of adsorbed copolymer on the carbon black particles, which are essentially incombustible under an inert atmosphere. Analytical centrifugation, optical microscopy, and transmission electron microscopy studies indicate that the star diblock copolymer acts as an effective flocculant at low concentration, with steric stabilization only being observed above a certain critical copolymer concentration (~5.5% w/w based on carbon black). This is attributed to the spatial location of the polystyrene block and the star copolymer architecture, which enables copolymer adsorption onto multiple carbon black particles at low coverage, leading to bridging flocculation. Above 5.5% w/w copolymer, the surface coverage is sufficiently high that all of the polystyrene "stickers" adsorb onto single carbon black particles, resulting in colloidally stable, sterically stabilized carbon black dispersions. Small-angle X-ray scattering (SAXS) is also used to characterize the copolymer-coated carbon black particles: this technique provides useful complementary insights regarding the rather subtle changes in the fractal morphology that occur with increasing copolymer concentration. Moreover, SAXS also provides direct evidence for the presence of the copolymer chains at the particle surface.

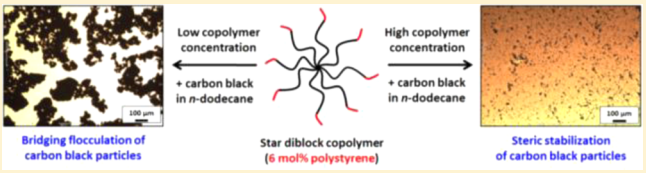

INTRODUCTION

It is well-documented that soluble polymers can influence the stability of colloidal dispersions via four different mechanisms: bridging flocculation, steric stabilization, depletion stabilization, and depletion flocculation.[1−12] The mechanism depends on the precise system and also on the polymer concentration. For example, bridging flocculation is normally associated with a relatively low polymer concentration, whereas steric stabilization or depletion effects are usually observed at higher polymer concentrations.[11,13,14] The first two mechanisms are particularly pertinent to the present study.

Ruehrwein and Ward first proposed the principle of bridging flocculation in 1952.[1] This phenomenon is now widely used for papermaking,[15] water treatment,[16] industrial effluent treatment,[17] and mining industries[18] to obtain efficient solid–liquid separations.[19] High molecular weight polymers have been shown to be particularly efficient bridging flocculants.[20] If the dimensions of the polymer chains are sufficiently large, then adsorption onto two or more particles can occur (see Figure 1a). This bridging aids particle aggregation, with strong kinetic effects being well-documented.[7,21,22] La Mer and Healy[23] reported that the degree of flocculation depended on both polymer molecular weight and dosage for the adsorption of polyacrylamides on calcium phosphate particles in aqueous media. Specific interactions such as hydrogen bonding have been demonstrated to enhance the extent of bridging flocculation.[24,25] It is also well-documented that increasing the polymer concentration can lead to initial bridging flocculation being supplanted by steric stabilization.[26,27] There are many literature reports of bridging flocculation based on the addition of high molecular weight water-soluble polymers such as poly(ethylene oxide) or polyacrylamide or poly(*N*-vinylpyrrolidone) to either silica sols

Received: March 11, 2015
Revised: May 11, 2015
Published: May 28, 2015

DOI: 10.1021/acs.macromol.5b00517
Macromolecules 2015, 48, 3691−3704

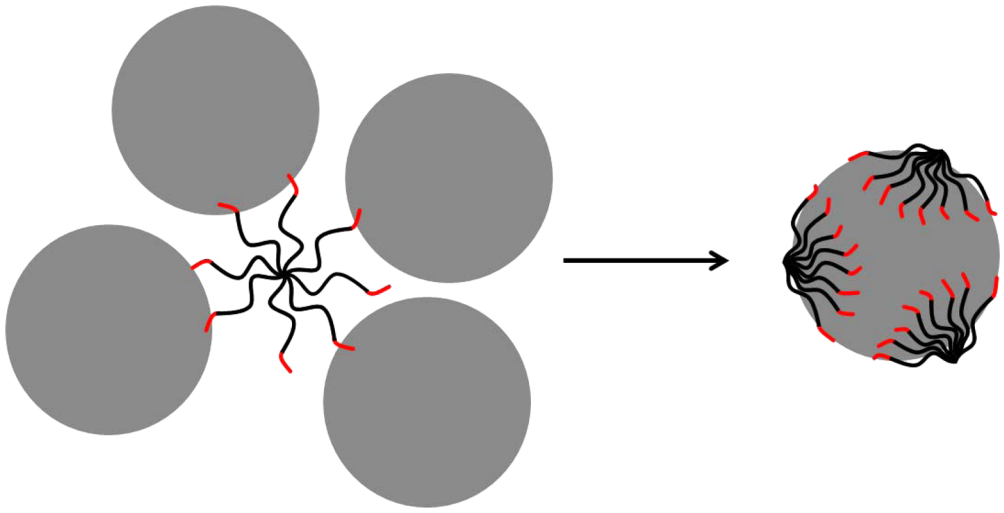

Figure 1. Schematic representation of the two roles played by the star diblock copolymer in the presence of a model colloidal substrate in nonpolar media: (a) bridging flocculant and (b) steric stabilizer. In practice, the carbon black particles utilized in this study exhibit a complex fractal morphology, rather than the simple spherical morphology depicted in this figure.

or polystyrene latex in *aqueous* media.[4,25,28,29] However, there appear to be rather few studies of bridging flocculation in *nonaqueous* media.[30,31] A rare example here is an early study by Hiemenz and Vold, who examined the kinetics of flocculation resulting from the adsorption of polystyrene onto carbon black particles from either toluene or cyclohexane.[7]

Steric stabilization is an important, generic, and highly versatile colloidal stabilization mechanism that is applicable for both aqueous and nonaqueous dispersions.[11] It has been widely utilized for many applications, including the preparation of inks,[32] latex paints,[33] and coatings,[34] the efficient dispersion of diesel soot in engine oils,[35] and the preparation of electrically conducting polymer particles.[36−40] The appropriate design of effective steric stabilizers requires an understanding of the interaction of the polymeric stabilizer with the particle surface, the continuous phase, and also the conformation that the adsorbed polymer chain adopts at the solid/liquid interface.[9,14] In particular, the polymeric stabilizer should be strongly adsorbed, provide high coverage of the particles, and form a thick, well-solvated steric barrier in order to offset the ever-present attractive van der Waals forces operating between colloidal particles.

Many different copolymer architectures are now accessible via so-called "living" polymerization chemistry, including homopolymers,[41,42] macromonomers,[43,44] statistical copolymers,[13,45,46] block copolymers,[47−49] graft copolymers,[50] and star copolymers.[51−53] All of these copolymer architectures have been examined as putative steric stabilizers for latex syntheses. The star diblock copolymer architecture is particularly relevant to the present study. Such copolymers have been utilized as drug carriers,[54] thermoresponsive gelators,[55−58] or viscosity modifiers in engine oil formulations.[59,60] The synthesis of star diblock copolymers has been achieved using anionic polymerization,[52] atom transfer radical polymerization,[61] or reversible addition−fragmentation chain transfer (RAFT) polymerization.[62] Alonzo et al.[21] recently reported the kinetics of adsorption of PS−PVP star diblocks onto a planar silicon surface from toluene. In the present study, we examine the influence of a commercial star diblock copolymer on the colloidal stability of carbon black particles in nonpolar media (e.g., *n*-dodecane). This copolymer comprises relatively long hydrogenated polyisoprene blocks as the inner cross-linked core, with relatively short polystyrene chains as the outer block. The adsorbed amount of copolymer, Γ, on the carbon black particles was determined indirectly via a supernatant depletion assay based on UV spectroscopy and also assessed directly by thermogravimetric analysis. Subsequently, the degree of dispersion of the carbon black particles was assessed as a function of copolymer concentration using analytical centrifugation, optical microscopy (OM), transmission electron microscopy (TEM), and small-angle X-ray scattering (SAXS).

EXPERIMENTAL SECTION

Materials. The star diblock copolymer used in this work is a commercial product that was supplied by BP Formulated Products Technology and was used as received. PAO2 base oil (a poly(α-olefin) synthetic Group 4 base oil, prepared via catalytic oligomerization of linear α-olefins) was selected for its similarity to *n*-dodecane and provided by BP Formulated Products Technology. Both *n*-dodecane and *n*-heptane were obtained from Fisher Scientific UK Ltd. Each solvent was used as received. Deuterated solvents for NMR studies were obtained from Goss Scientific Ltd., UK, and were used as received. The carbon black (Regal 250-R grade) was kindly supplied by Cabot Plastics (Billerica, MA) and was used as received.

Gel Permeation Chromatography. The molecular weight distribution of the star diblock copolymer was assessed by gel permeation chromatography (GPC) using THF eluent. The THF GPC setup was equipped with two 5 μm "Mixed C" 30 cm columns, a Varian 290-LC pump, and a WellChrom K-2301 refractive index detector operating at 950 ± 30 nm. The THF mobile phase contained 2.0% v/v triethylamine and 0.05% w/v butylhydroxytoluene (BHT), and the flow rate was fixed at 1.0 mL min^{-1}. A series of ten near-monodisperse polystyrene standards (M_n = 580 to 552 500 g mol^{-1}) were used for calibration.

Dynamic Light Scattering (DLS). Hydrodynamic diameters were measured at 25 °C using a Malvern Zetasizer NanoZS model ZEN 3600 instrument equipped with a 4 mW He−Ne solid-state laser operating at 633 nm. Backscattered light was detected at 173°, and the mean particle diameter was calculated from the quadratic fitting of the correlation function over 30 runs of 10 s duration.

DOI: 10.1021/acs.macromol.5b00517
Macromolecules 2015, 48, 3691−3704

All measurements were performed three times and data were analyzed using CONTIN software.

Transmission Electron Microscopy. Studies were conducted using a Phillips CM100 microscope operating at 100 kV on unstained samples prepared by drying a drop of dilute sample (approximately 0.01 wt %) on a carbon-coated copper grid.

Small-Angle X-ray Scattering (SAXS) Studies. SAXS patterns were collected at a synchrotron source (Diamond Light Source, station I22, Didcot, UK) using monochromatic X-ray radiation and a 2D Pilatus 2 M CCD detector (wavelength λ = 0.10 nm, camera length = 10 m, which gives a q range from 0.011 to 1.33 nm^{-1}, where $q = 4\pi \sin\theta/\lambda$ is the length of the scattering vector and θ is half of the scattering angle). A liquid cell comprising two mica windows each of 25 μm thickness attached by an adhesive double-sided tape to both sides of a polycarbonate washer of 1 mm thickness was used as a sample holder. Carbon black dispersions (1.0% w/w solids; 1−10% copolymer based on the mass of carbon black) were loaded into the partially assembled cell (a mica window attached to one side of the washer), and then the dispersion was sealed in the cell by attaching the second mica window to the washer. In order to avoid sedimentation of the carbon black on the time scale of the SAXS experiments, the loaded liquid cell was continuously rotated by a motor. Scattering data were reduced (i.e., integrated, normalized, and background-subtracted) by Dawn software developed at Diamond Light Source and were further analyzed using Irena SAS macros for Igor Pro.[63]

^{1}H NMR spectroscopy. The mean polystyrene content of the diblock copolymer dissolved in a nonselective solvent ($CDCl_3$) was determined using a Bruker AV1-250 MHz NMR spectrometer (64 scans per spectrum). Variable temperature spectra were recorded between 25 and 100 °C using d_{26}-dodecane using a Bruker AV1-400 MHz NMR spectrometer (32 scans per spectrum).

UV Spectroscopy. UV spectra were recorded at 20 °C for the diblock copolymer dissolved in *n*-dodecane using a PerkinElmer Lambda 25 instrument operating between 200 and 500 nm. A linear calibration curve was constructed for the same copolymer dissolved in pure chloroform at a fixed wavelength of 262 nm, which corresponds to the aromatic chromophore of the polystyrene block. This gave a molar extinction coefficient of 222 ± 2 mol^{-1} dm^3 cm^{-1}, which is close to the literature value reported for polystyrene.[64]

Copolymer Adsorption onto Carbon Black via Supernatant Depletion Assay Using UV Spectroscopy. The desired mass of diblock copolymer (3.0−90.0 mg) was weighed into a glass vial, and carbon black (300.0 mg) was weighed into a separate vial. Then *n*-alkane (5.00 mL) was added, followed by stirring at 20 °C (Turrax stirrer, 1 min, 2500 rpm). The resulting star copolymer dispersion was added to the preweighed carbon black, stirred (Turrax stirrer, 1 min, 2500 rpm), sonicated for 1 h, and then left on a roller mill for 16 h overnight. The resulting dispersion was centrifuged for 4 h at 18 000 rpm in a centrifuge rotor that was precooled to 15 °C so as to minimize solvent evaporation. Taking care not to disturb the sedimented carbon black particles, the supernatant was decanted into an empty vial, and then 0.80 mL of this solution was analyzed by UV spectroscopy. The aromatic chromophore at 262 nm due to the polystyrene block was used to quantify the copolymer concentration remaining in the supernatant after exposure to the carbon black, thus enabling the adsorbed amount to be determined by difference.

Thermogravimetric Analysis. Analyses were conducted on the pristine star diblock copolymer, carbon black alone, and star copolymer-coated carbon black particles. Each sample was heated under a nitrogen atmosphere up to 800 °C at a heating rate of 10 °C min^{-1} using a Q500 TGA instrument (TA Instruments). The mass loss observed between 300 and 500 °C was attributed to complete pyrolysis of the diblock copolymer, with the remaining incombustible residue being attributed to carbon black.

Analytical Centrifugation. Carbon black aggregate diameters were determined using a LUMiSizer analytical photocentrifuge (LUM GmbH, Berlin, Germany) at 20 °C. Measurements were conducted on carbon black dispersions (10% w/w solids; 1−10% copolymer based on the mass of carbon black) in either *n*-dodecane or d_{26}-dodecane at 200−4000 rpm using 2 mm path length polyamide cells. The particle density is an essential input parameter for analytical centrifugation studies. In the present case, the effective carbon black density is significantly reduced because of the presence of the adsorbed star copolymer. Thus, this parameter was determined using Stokes' law by performing LUMiSizer analyses in both *n*-dodecane and d_{26}-dodecane (see later for further details). The LUMiSizer is a microprocessor-controlled analytical centrifuge and is particularly convenient for the analysis of diblock copolymer-stabilized carbon black dispersions described in this work, since it allows simultaneous characterization of multiple dispersions in organic solvents over a wide range of operating temperature (4−60 °C). The LUMiSizer employs STEP-Technology (space- and time-resolved extinction profiles) allowing the measurement of the intensity of transmitted light as a function of time and position over the entire cell length simultaneously. The progression of these transmission profiles contains information on the rate of sedimentation and, given knowledge of the particle density, enables assessment of the particle size distribution.

Optical Microscopy. 10 wt % carbon black dispersions were placed on a microscope slide and covered with a coverslip. Digital images were recorded using a Motic DMBA300 digital biological microscope equipped with a built-in camera and Motic Images Plus 2.0 ML software.

Viscometry. These studies were conducted using an Ostwald viscometer immersed in a water bath at 20 °C. Each measurement was repeated five times, and the data were averaged. The solution viscosity was calculated from the viscosity of a known solvent.

X-ray Photoelectron Spectroscopy. Studies were conducted on carbon black pressed onto indium foil using a Kratos Axis Ultra DLD X-ray photoelectron spectrometer equipped with a monochromatic Al X-ray source ($h\nu$ = 1486.6 eV) operating at 6.0 mA and 15 kV at a typical base pressure of 10^{-8} Torr. The step size was 1.0 eV for all survey spectra (pass energy = 160 eV). Spectra were typically acquired from at least two separate sample areas.

RESULTS AND DISCUSSION

THF GPC analysis of the commercial star diblock copolymer used in this study indicated an M_n of 384 000 g mol^{-1} and an M_w/M_n of approximately 1.40 (expressed relative to a series of near-monodisperse polystyrene calibration standards) (see Figure S1). Such copolymers can be prepared by anionic polymerization via the "arm-first method" using sequential monomer addition.[60] Thus, styrene was polymerized first, followed by isoprene and the divinylbenzene cross-linker. Based on formulations disclosed in the patent literature,[60] it is estimated that each star comprises approximately eight diblock copolymer arms. According to ^{1}H NMR analysis conducted in $CDCl_3$ (see Figure S2), there was little or no evidence for unsaturated vinyl groups on the polyisoprene chains, which suggests that the copolymer had been subjected to catalytic hydrogenation. One method for achieving such a high level of saturation is to use hydrogen gas with a Ni(octanoate)$_2$ catalyst and an $AlEt_3$ cocatalyst in cyclohexane at 65 °C.[60] Integrating the assigned signals in the same ^{1}H NMR spectrum enables the mean polystyrene content of this star diblock copolymer to be calculated as approximately 6 mol %. These relatively short blocks comprise the outer arms of the star copolymer and are expected to be rather poorly solvated in *n*-alkanes.[65] Hence, a micellar gel network is formed at relatively high copolymer concentrations (see Figure S3). At lower copolymer concentrations, this star copolymer acts as a viscosity modifier (or thickener), which is its primary function as an additive in commercial engine oils.[60] In the context of the present work, when the star copolymer is added to carbon black particles in *n*-alkanes, it is assumed that the polystyrene blocks act as "stickers" that aid copolymer adsorption onto the carbon black (see Figure 1), which is known to be a useful mimic for diesel engine soot.[35,66−69]

DOI: 10.1021/acs.macromol.5b00517
Macromolecules 2015, 48, 3691−3704

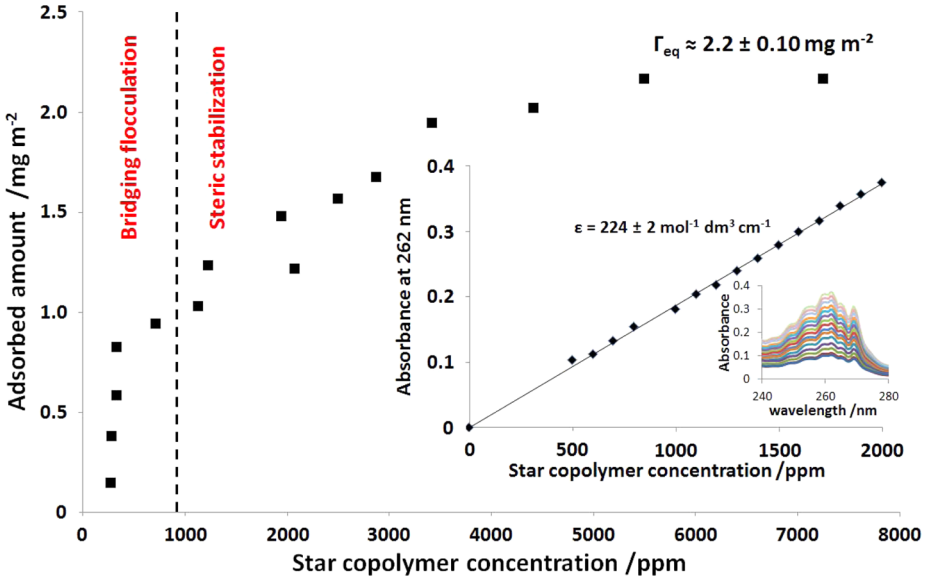

Figure 2. Low-affinity Langmuir-type adsorption isotherm obtained at 20 °C for the star diblock copolymer adsorbed onto carbon black from *n*-dodecane, as determined using a supernatant depletion assay based on UV spectroscopy. The insets show the Beer−Lambert calibration plot used to determine the star copolymer concentration in each supernatant and the original UV spectra used to construct this calibration plot.

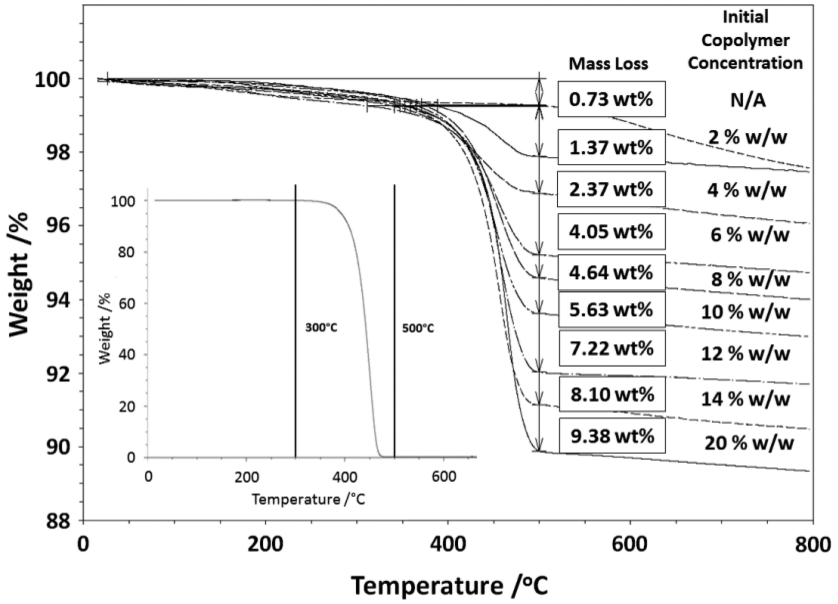

Figure 3. Thermogravimetric curves obtained for the adsorption of increasing amounts of star diblock copolymer onto carbon black particles from *n*-dodecane at 20 °C. Analyses were performed under a nitrogen atmosphere at a heating rate of 10 °C/min. Carbon black loses only 0.73 mass % when heated up to 500 °C. In contrast, the star diblock copolymer (see inset curve) is completely pyrolyzed under these conditions. Thus, the observed mass loss at 500 °C for star diblock copolymer-coated carbon black particles can be attributed to the copolymer content (after correcting for the carbon black mass loss). This direct method for determining the adsorbed amount of star diblock copolymer is in reasonably good agreement with the indirect supernatant assay method based on UV spectroscopy (see two adsorption isotherms shown in Figure S8).

A representative transmission electron micrograph of the commercial carbon black (Regal 250 R) employed in this study confirms its characteristic fractal morphology (see Figure S4). According to our earlier study,[70] BET surface area analysis (N_2 adsorbate at 77 K) indicated a specific surface area of 43 m g^{-1} for this material. Combined with a solid-state density of 1.89 g cm^{-3} determined by helium pycnometry,[70] this suggests a mean sphere-equivalent diameter of approximately 74 nm, which corresponds to the mean grain size for this particular carbon black. Furthermore, X-ray photoelectron spectroscopy (XPS) studies revealed the presence of low levels of both sulfur (~0.50 atom %) and oxygen (~0.94 atom %) at the surface of this colloidal substrate (see Figure S5). The extent of copolymer adsorption onto this model colloidal substrate from *n*-dodecane at 20 °C was examined indirectly using a supernatant depletion assay based on UV spectroscopy, after centrifugal sedimentation of the relatively dense carbon black particles. Here the polystyrene block acts as a convenient aromatic UV chromophore, since it gives rise to a strong signal at 262 nm and a highly linear Beer−Lambert law plot (see inset in Figure 2). In this case, and in contrast to our earlier related study,[70] the supernatant assay was performed directly in *n*-dodecane since there was negligible

DOI: 10.1021/acs.macromol.5b00517
Macromolecules 2015, 48, 3691−3704

scattering from the molecularly dissolved copolymer. An adsorption isotherm was constructed using this protocol (see Figure 2).

Langmuir-type adsorption is observed, as generally expected for polymer adsorption.[71] The maximum adsorbed amount of copolymer, Γ (corresponding to monolayer coverage), can be calculated from the linear form of the Langmuir equation.[72] This parameter was found to be somewhat solvent-dependent, with Γ values of 2.2 ± 0.1, 3.1 ± 0.1, and 2.1 ± 0.1 mg m^{-2} being obtained for *n*-dodecane, *n*-heptane, and PAO2 base oil respectively (see Figures S6 and S7). These adsorbed amounts are relatively high for merely physical adsorption.[73] In addition, thermogravimetric analysis (TGA) was used to determine the amount of adsorbed copolymer on the carbon black surface from *n*-dodecane (see Figure 3). A control experiment confirmed that minimal mass loss (~0.73%) occurred for carbon black particles alone on heating up to 500 °C under an inert atmosphere. In contrast, the star diblock copolymer was fully pyrolyzed under these conditions (see inset thermogram in the same figure). Thus, pyrolysis of the copolymer-coated carbon black particles (isolated as compacted sediments after centrifugation) allowed the adsorbed amount of copolymer to be determined. A series of thermograms are shown in Figure 3; higher mass losses are observed at 500 °C as the initial copolymer concentration is gradually increased.

Adsorption isotherms constructed using each technique are shown in Figure S8. When assessed using TGA, the apparent adsorbed amount continues to increase beyond the monolayer coverage value indicated by UV spectroscopy. This is because the star diblock copolymer is not fully molecularly dissolved in *n*-dodecane. Indeed, DLS studies (see Figure S9) indicate that some degree of self-association occurs in dilute solution in this solvent, which is presumably mediated by attractive forces between the partially solvated polystyrene chains. Control experiments confirm that a minor fraction of the star diblock copolymer can be sedimented under the centrifugation conditions used to isolate the carbon black particles prior to TGA analysis. Thus, the TGA technique should be reliable below (and up to) monolayer coverage, since there is essentially no excess copolymer in the supernatant in this regime. However, it tends to *overestimate* the adsorbed amount of copolymer when the latter is present in excess. Similarly, the supernatant depletion assay based on UV spectroscopy must *underestimate* the adsorbed amount of copolymer above monolayer coverage. In summary, these two techniques report consistent data for adsorbed amounts up to monolayer coverage but necessarily diverge thereafter.

Optical microscopy, TEM, and analytical centrifugation were used to determine the boundary between bridging flocculation and steric stabilization of the carbon black particles as a function of copolymer concentration (see Figures 4 and 5). Inspecting Figure 4, large agglomerates can be observed at 5.0% w/w copolymer based on carbon black. OM and TEM are sensitive to different length scales: the former technique is sensitive to the presence of strongly light-absorbing micron-sized carbon black mass fractals, whereas the latter technique enables the population of well-dispersed submicron-sized carbon black "fines" to be visualized. At (or above) 10% w/w copolymer, a few large agglomerates are still present, but mainly smaller aggregates are observed along with some primary particles, suggesting reasonably stable dispersions.

At lower copolymer concentrations, it is postulated that the star copolymer adsorbs simultaneously onto multiple carbon black particles via its outer polystyrene blocks, thus promoting

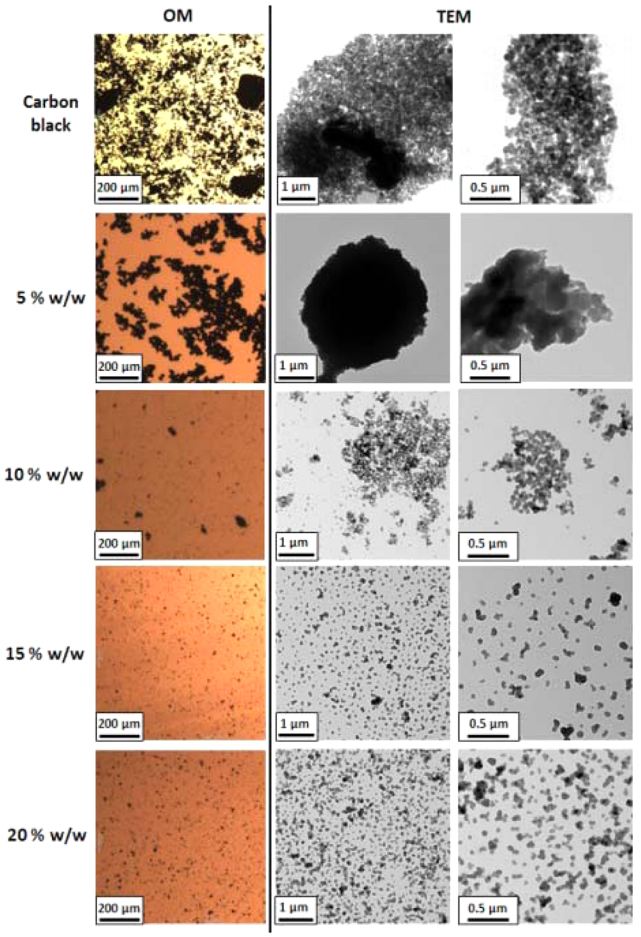

Figure 4. Representative TEM images obtained for carbon black particles in the presence of 5–20% w/w star diblock copolymer in *n*-dodecane. The corresponding optical microscopy images recorded for these four dispersions are also shown; these images confirm that a much greater degree of dispersion is obtained at higher copolymer concentration. This is because the star diblock copolymer switches from acting as a bridging flocculant to acting as an effective steric stabilizer at a certain critical concentration (see Figure 1).

bridging flocculation.[74] At higher copolymer concentrations, the star copolymer instead acts as a steric stabilizer, resulting in colloidally stable carbon black dispersions (see Figure 1b). This behavior differs qualitatively from that reported to a hydrogenated polyisoprene–polystyrene *linear* diblock copolymer, for which only steric stabilization is observed via micellar adsorption.[70] However, it can be dangerous to infer too much regarding the apparent degree of dispersion of particles using *post mortem* TEM studies because drying artifacts can sometimes occur. Thus, selected carbon black dispersions were also characterized using analytical centrifugation (see below) and SAXS (see later).

In order to calculate particle size distributions via analytical centrifugation, the particle density is required. The solid-state density of carbon black has been determined to be 1.89 g cm^{-3}, as judged by helium pycnometry.[70] However, its *effective* particle density in the present case is significantly reduced because the density of the solvated layer of adsorbed copolymer chains is comparable to that of the solvent, which is much less dense than carbon black. Thus, Stokes' law was utilized in order to determine the effective particle density.[75] In principle, centrifugation of two copolymer-adsorbed carbon black dispersions prepared in two

DOI: 10.1021/acs.macromol.5b00517
Macromolecules 2015, 48, 3691–3704

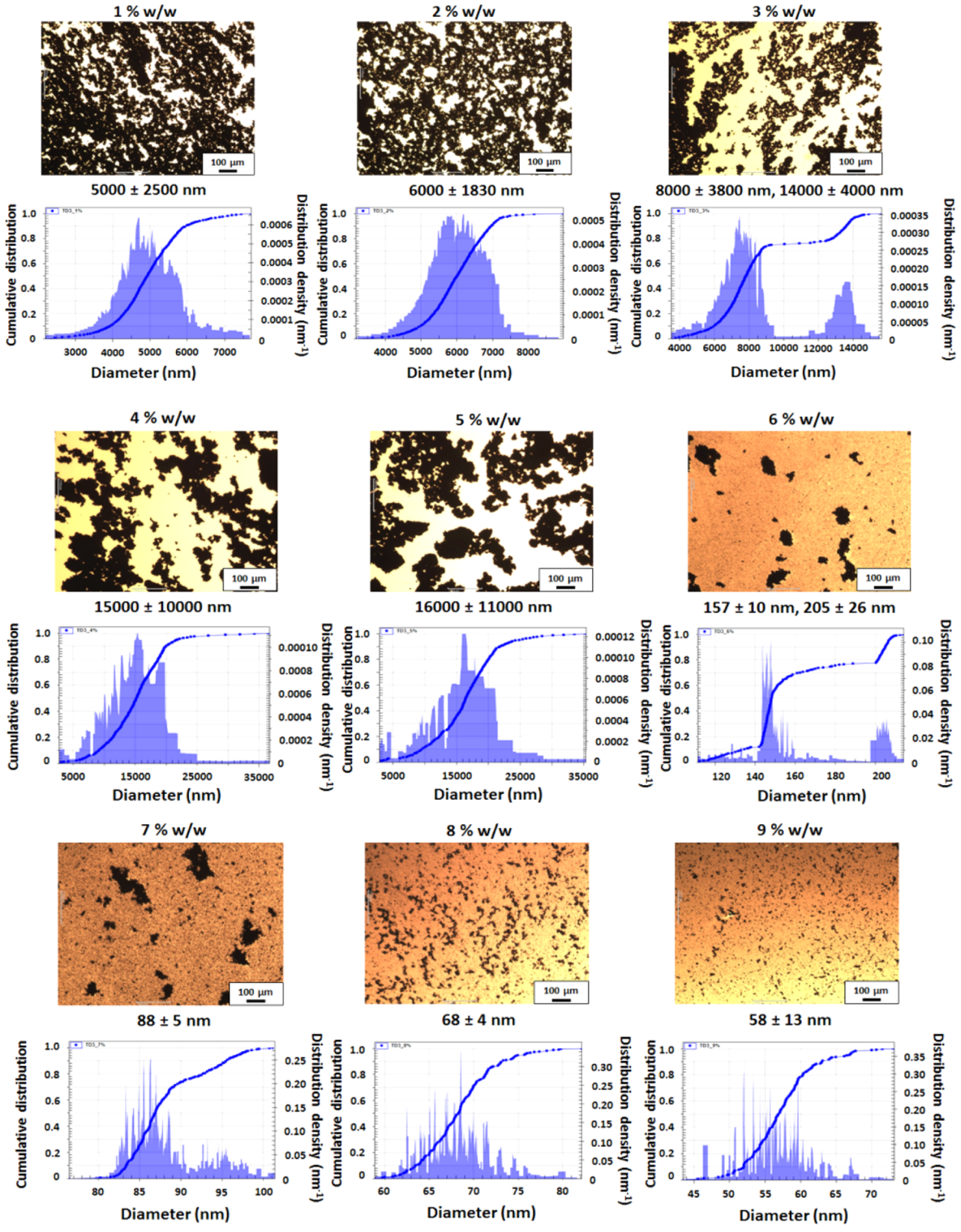

Figure 5. Representative optical microscopy images obtained for carbon black dispersions prepared using 1−9% w/w star diblock copolymer in *n*-dodecane at 20 °C. The corresponding particle size distributions (and mean volume-average particle diameters) determined via analytical centrifugation (LUMiSizer instrument) are also shown for each dispersion.

comparable solvents with differing densities and viscosities (in this case, *n*-dodecane and d_{26}-dodecane) should produce two different particle velocities v_1 (or v_2):

$$v_1 = \frac{(\rho_p - \rho_{F,1})X^2\omega^2}{18\eta_1}r \quad (1)$$

$$v_2 = \frac{(\rho_p - \rho_{F,2})X^2\omega^2}{18\eta_2}r \quad (2)$$

Here ρ_p is the effective particle density, $\rho_{F,1}$ (or $\rho_{F,2}$) is the solvent density, η_1 (or η_2) is the solvent dynamic viscosity, ω is the angular velocity, X is the sedimentation position of the particles,

DOI: 10.1021/acs.macromol.5b00517
Macromolecules 2015, 48, 3691−3704

and r is the overall mean radius of the copolymer-coated carbon black particles. Combining eqs 1 and 2 to eliminate the experimental constants X, ω, and r and rearranging terms leads to an expression for the effective density of the copolymer-coated carbon black particles, ρ_p:

$$\rho_p = \frac{v_1\eta_1\rho_2 - v_2\eta_2\rho_1}{v_1\eta_1 - v_2\eta_2} \quad (3)$$

Unfortunately, the solution dynamic viscosity of d_{26}-dodecane (in this formalism, η_2) is not available in the literature. Thus, Ostwald (capillary) viscometry was used to determine the kinematic viscosity, υ, of d_{26}-dodecane relative to that of n-dodecane at 20 °C (see Supporting Information, Table S1). This kinematic viscosity was converted to the corresponding dynamic viscosity using eq 4.

$$\upsilon = \frac{\mu}{\rho} \quad (4)$$

Here υ is the kinematic viscosity, μ is the dynamic viscosity, and ρ is the solvent density. Using this approach, the dynamic viscosity of d_{26}-dodecane was calculated to be 1.44 mPa·s. This experimental value agrees very well with that determined using an empirical relationship derived by Lutskii for the relative viscosities of deuterated n-alkanes compared to the equivalent protonated compounds.[76,77]

Using eq 3, an effective particle density, ρ_p, of 0.98 ± 0.01 g cm^{-3} was estimated for star copolymer-stabilized carbon black particles dispersed in n-dodecane at 20 °C prepared using 10% w/w copolymer based on carbon black (see Supporting Information for details; these conditions were selected since they correspond to approximately monolayer coverage of the carbon black particles; see Figure 2). This appears to be a reasonable value, since it enables a mean volume-average diameter of 70−75 nm to be calculated for these sterically stabilized carbon black particles via analytical centrifugation. This size seems physically realistic because it is close to the mean grain size for carbon black, which is estimated to be around 74 nm by BET surface area analysis.[70] It is worth emphasizing here that the relatively small error of ±0.01 g cm^{-3} in ρ_p actually leads to an error of around ±5% in the volume-average particle diameter, since it is the *difference* between the effective particle density (0.98 g cm^{-3}) and the spin fluid (0.78 g cm^{-3}) that is employed in the LUMiSizer analysis. All particle size distributions determined by analytical centrifugation in this study were calculated using the above effective particle density. Clearly, this approximation most likely introduces systematic errors when working in solvents other than n-dodecane, especially at temperatures other than 20 °C and copolymer concentrations other than 10% w/w. However, determination of effective particle densities under all of these conditions was beyond the scope of this work.

To assess the precise location of the flocculation/dispersion boundary in a given solvent, analytical centrifugation was used to determine mean diameters for the carbon black aggregates. In this context, a smaller apparent size indicates a higher degree of dispersion. In principle, analytical centrifugation can be used to assess the relative populations of both the micron-sized agglomerates (mass fractals) and also the submicron-sized aggregates/primary particles. Figure 5 compares the optical micrographs obtained for copolymer-stabilized carbon black dispersions in n-dodecane with the equivalent analytical centrifugation particle size distribution plots. The flocculation/dispersion boundary is discernible at around 5−6% w/w copolymer for both techniques. The average floc size increases as this critical concentration is approached, presumably as initial aggregates combine to form larger agglomerates. Indeed, the bimodal distribution observed at 3% w/w copolymer via analytical centrifugation provides some evidence for the coexistence of these two species. Similarly, the bimodal size distribution observed at 6.0% w/w copolymer (i.e., just beyond the flocculation/dispersion boundary) indicates the presence of a few remaining carbon black agglomerates together with a major population of rather smaller aggregates. Finally, at 8−9% w/w copolymer, the mean carbon black particle size is close to the mean grain size of 74 nm indicated by BET studies.[70]

Compared to related techniques such as disk centrifuge photosedimentometry, one important advantage of the LUMiSizer instrument is that it enables experiments to be performed over a wide range of temperature, rather than just ambient temperature. Accordingly, similar copolymer concentration-dependent studies were conducted using n-heptane, n-dodecane, or PAO2 base oil at 4, 20, and 60 °C. Inspecting Figure 6, the critical copolymer concentration corresponding to the flocculation/dispersion phase boundary is more or less independent of temperature. However, this parameter is clearly solvent-dependent, being around 7−8% w/w for n-heptane, 5−6% w/w for n-dodecane, and approximately 6−7% w/w for PAO2 base oil. As stated above, a somewhat higher affinity adsorption isotherm is observed for n-heptane compared to that found for n-dodecane and PAO2 base oil (see Figure S6). Using these three Γ values, the critical fractional coverage, θ_c, corresponding to the flocculation/dispersion boundary was calculated for each solvent. For n-heptane, n-dodecane, and PAO2, θ_c is estimated to be 0.48 ± 0.01, 0.45 ± 0.02, and 0.60 ± 0.02, respectively. The difference in θ_c for the first two solvents is within experimental error, whereas the higher fractional coverage observed for the PAO2 suggests a somewhat higher degree of solvation for the star copolymer in this base oil.

Returning to Figure 6, higher dispersion stabilities (as judged by smaller apparent particle diameters) were always observed at 4 °C compared to those at 20 °C, whereas poorer stabilities were universally obtained at 60 °C. To examine whether the star diblock copolymer *alone* exhibits temperature sensitivity, variable temperature ^{1}H NMR studies were performed from 25 to 100 °C for this copolymer dissolved in d_{26}-dodecane (Figure 7).

An apparent polystyrene content of 3.2 ± 0.2 mol % was observed at 25 °C. As stated earlier, ^{1}H NMR analysis in $CDCl_3$, which is a good solvent for both the polystyrene and hydrogenated polyisoprene blocks, indicates that the actual polystyrene content of this copolymer is 6 mol %. This observation indicates that the outer polystyrene blocks of the star copolymer are only *partially* solvated (see Figure S2). This is consistent with the ability of this nonlinear copolymer to act as an effective bridging flocculant. However, there is surprisingly little change in the apparent polystyrene content of this copolymer with temperature.

The temperature-dependent intrinsic viscosity of a polyisobutylene succinimide (PIBSI) dispersant was studied by Won et al.[67] These authors found that raising the temperature caused a reduction in solvation of the PIBSI chains. This compromises the efficiency of this dispersant in preventing the agglomeration of carbon blacks in n-alkanes at elevated temperature. In the context of the present study, it is hypothesized that hydrogenated polyisoprene chains may also become less solvated at higher temperatures, which would account for the inferior dispersion stability observed in the LUMiSizer experiments performed at 60 °C.

DOI: 10.1021/acs.macromol.5b00517
Macromolecules 2015, 48, 3691−3704

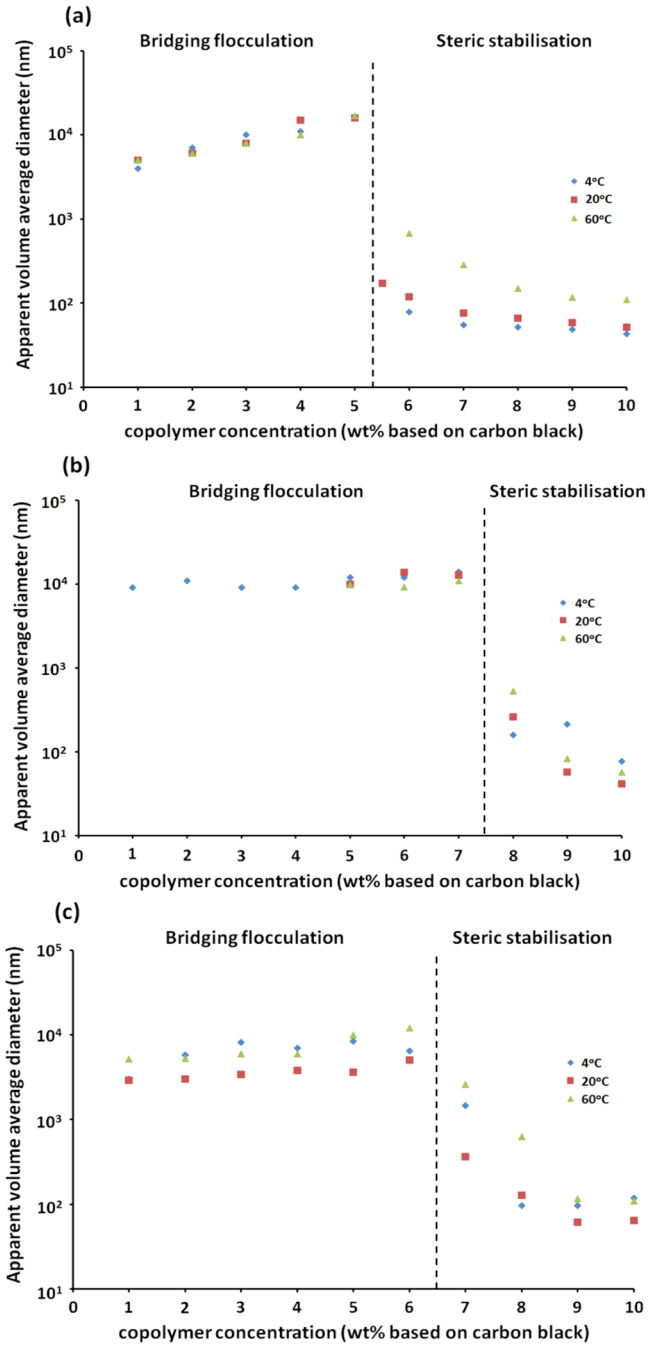

Figure 6. Concentration dependence of the mean volume-average diameter for dispersions of carbon black particles dispersed in (a) *n*-dodecane, (b) *n*-heptane, and (c) PAO2 base oil in the presence of star diblock copolymer, as determined via analytical centrifugation (LUMiSizer instrument) at 4, 20, and 60 °C.

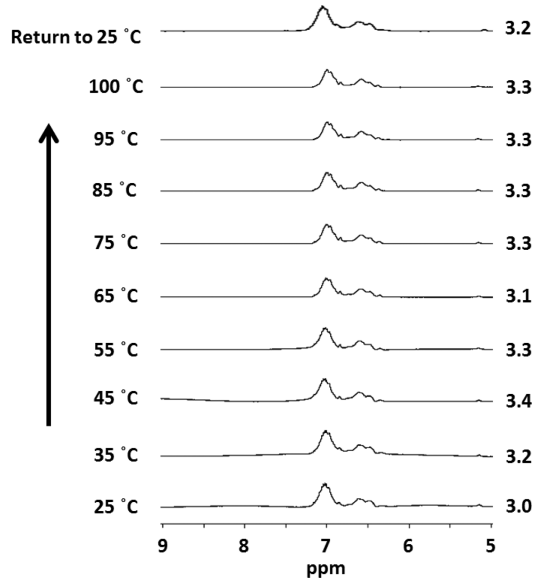

Figure 7. Partial ^{1}H NMR spectra recorded for the star diblock copolymer in d_{26}-dodecane on heating from 25 to 100 °C, followed by cooling to 25 °C. The appearance of aromatic signals is attributed to partial solvation of the polystyrene outer arms of the star diblock copolymer. The *apparent* polystyrene content (in mol %) of the star diblock copolymer is indicated at the right-hand side of each spectrum; the actual polystyrene content is ~6 mol %.

SAXS Analysis. It is well-known that the structural morphology of carbon black (and soot) particles can be described as a hierarchy composed of five species: fractal agglomerates (1) at the micron length scale, aggregates (2) and primary particles (3) at the nanometer scale, subunits (4) (a turbostratic structure comprising graphite-like layers arranged in nonaligned basal planes) at the sub-nanometer scale, and finally graphite-like carbon layers (5) at the atomic scale.[78−82] The first three structural levels can be analyzed by SAXS/USAXS (ultrasmall-angle X-ray scattering), while the other two levels can be characterized using wide-angle X-ray scattering (WAXS). The primary particles are fused together to form aggregates that are considered to be unbreakable via dispersion processes,[81] but the larger hierarchical structures can be affected by the processing conditions.[78,83,84] Thus, SAXS/USAXS measurements are often employed for characterization of carbon black/soot dispersions.[81,84,85] In this context, the unified Guinier plus power law empirical model proposed by Beaucage (unified fit)[85−88] is commonly employed since it enables an arbitrary number of interrelated structural features at various length scales to be described.[81,89] The scattering profile is decomposed into the scattering intensity, $I(q)$, arising from each structural element comprising the hierarchical structures. It can be expressed analytically as follows:

$$I(q) \cong \sum_{i=1}^{N}\left[G_i \exp\left(-\frac{q^2 R_{g,i}{}^2}{3}\right) + \exp\left(-\frac{q^2 R_{g,i+1}{}^2}{3}\right) B_i \times \left(\frac{[\mathrm{erf}(qk_i R_{g,i}/\sqrt{6}]^3}{q}\right)^{P_i}\right] S_i(q) \quad (5)$$

where N is the number of structural elements/levels, and the scattering intensity originating from each structural element/level (i.e., the expression enclosed by the square brackets) is represented as the sum of two components describing the Guinier and power laws, respectively. G_i is the Guinier pre-exponential factor of the ith structural element, and B_i is a constant that is characteristic of the type of power-law scattering, as defined by the regime in which the exponent P_i falls. $R_{g,i}$ and $R_{g,i+1}$ are radii of gyration of a large-scale structure and a small-scale substructure, respectively. The exponent term associated with $R_{g,i+1}$ provides a high q cutoff for the power law component, which is incorporated into eq 5 in order to describe scattering from a system with inter-related multiscale features. This factor is commonly used for mass fractals.[63,87] If the latter is not required,

DOI: 10.1021/acs.macromol.5b00517
Macromolecules 2015, 48, 3691−3704

the exponent term is assumed to be unity. P_i is a scaling exponent of the power law assigned to the larger structure $R_{g,i}$. P_i is a scaling exponent of the power law assigned to the larger structure $R_{g,i}$. Generally, the value of the exponent enables the structural morphology to be classified. Thus, for mass fractals $P_i < 3$, for surface fractals $3 < P_i < 4$, for Porod's law (smooth surface with a sharp interface) $P_i = 4$ and for diffuse interfaces $P_i > 4$ (negative Porod's law deviation). k_i is an empirical constant that has either a value of unity for steep power law decays ($P_i > 3$) or 1.06 for mass fractals ($1.5 < P_i < 3$).[87]

The model indicated by eq 5 assumes that four parameters (G, R_g, B, and P) describing each hierarchical level are allowed to vary independently. This can create undesired artifacts that could, for example, show up as kinks in the fitted curve.[90] However, it is required to provide sufficient flexibility for the model, especially when analyzing a polydisperse system with an ill-defined morphology (e.g., carbon black). Based on some assumptions for the structural model, the number of independent parameters can be reduced to three (G, R_g, and P), as it has been demonstrated originally for Gaussian chains (for $P = 2$)[87] or in a more general form for the polymer fractal model.[90] Introducing this parameter constraint makes the Beaucage model more reliable for a particular case but also makes this method inapplicable for more general analysis when the structure is unknown. This situation has been unambiguously demonstrated by comparing the performance of the constrained Beaucage model for SAXS analysis of polymer mass fractals and spherical micelles. Reasonable results are produced in the former case, but the expected power law exponent value was not obtained in the latter case.[90] Thus, a more generic version of the unified fit, based on four parameters for each level, was employed in this work. This allows a broader range of data to be fitted, but may produce physically unreasonable results when the volume parameters (G and R_g) and the surface parameters (B and P) of the fitting curve do not match each other (e.g., for a situation with either too much or too little surface for a given volume). Useful criteria for checking the validity of the fitted data are incorporated in the Irena macros for Igor Pro.[63] A validity parameter, f_i, calculated from fitting results is given by

$$f_i = (B_{q_{1,i}} - G_{q_{1,i}})/G_{q_{1,i}} \quad (6)$$

where $G_{q_{1,i}} = G_i \exp(-{q_{1,i}}^2 {R_{g,i}}^2/3)$ and $B_{q_{1,i}} = B_i/{q_{1,i}}^{P_i}$ are numerical values of the Guinier and power law components of the Beaucage model, respectively, at a rollover q value $q_{1,i} = 2/R_{g,i}(P_i/2)^{1/2}$. This expression for q is similar to the definition of the point in the Guinier−Porod model at which the Guinier and Porod terms and their derivatives are continuous, $q = 1/R_g(3P/2)^{1/2}$.[90] f_i remains constant for both the Guinier−Porod model and the constrained Beaucage model; depending on the rollover q value, f_i is either zero or close to zero. As a crude estimate, it is assumed in the Irena macros that an empirical Beaucage model fit is physically reasonable if the validity parameter lies within the interval $-0.633 < f_i < 2.25$. These limits assume the conversion of a unified fit into a log-normal size distribution.[91] For example, a situation whereby $B_{q_{1,i}} > G_{q_{1,i}}$ (corresponding to $f_i < 0$; see eq 6) may occur if there are interparticle interactions, whereas $B_{q_{1,i}} < G_{q_{1,i}}$ (corresponding to $f_i > 0$; eq 6) may occur if the system has a sufficiently broad size distribution. However, it is emphasized that the f_i limits are merely a guide, rather than a strict rule for the empirical Beaucage model. There will be cases when physically meaningless fits may be obtained within the validity interval. Similarly, physically realistic fits may be produced outside of these limiting values.

Weakly correlated particles can also be considered using eq 5 by incorporating a structure factor, $S_i(q)$,[88,92] which comprises a damped spherical correlation of colloidal particles:

$$S_i(q) = [1 + \eta_i f(qR_{c,i})]^{-1} \quad (7)$$

where $f(qR_{c,i}) = 3[\sin(qR_{c,i}) - qR_{c,i}\cos(qR_{c,i})]/(qR_{c,i})^3$ is the form factor for spherical interactions correlated over a distance R_c and η describes the degree of correlation, which is assumed to be weak if $\eta < 3$. If no correlations are present for the ith structural element/level, then $S_i(q) = 1$. The multilevel unified fit, eq 5, is implemented as a routine in the SAXS data analysis software Irena SAS macros for Igor Pro.[63]

Three hierarchical structures can be identified in the SAXS pattern recorded for the original carbon black dispersed in n-dodecane (see Figure 8, the lowest pattern). By analogy with

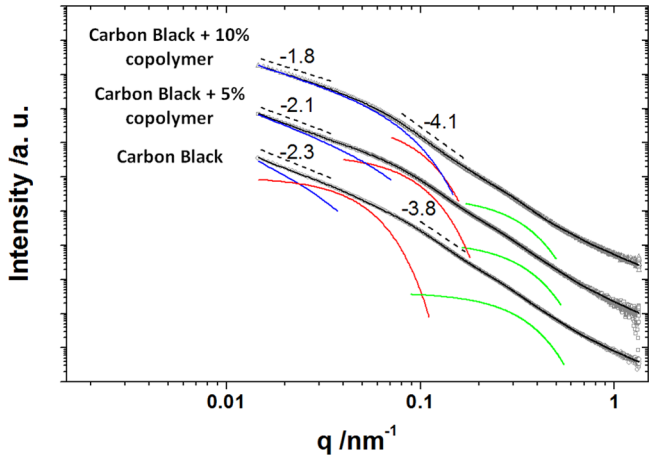

Figure 8. Representative SAXS patterns recorded for a 1.0% w/w carbon black dispersion in n-dodecane alone (circles) and in n-dodecane at two star diblock copolymer concentrations (5.0% w/w based on carbon black, squares; 10.0% w/w based on carbon black, triangles). Dashed lines indicate the power law gradient of the scattering intensity. Solid black lines show multilevel unified fits to the data. Colored lines indicate unified fits to the mass fractals (blue) and the Guinier components of the unified fits to both the agglomerates (red) and the primary particles (green).

previous work,[85] the SAXS intensity gradient of −2.3 for $q < 0.03$ nm^{-1} is associated with mass fractals formed by carbon black aggregates, and the corresponding gradient of −3.8 for 0.1 nm^{-1} $< q < 0.2$ nm^{-1} is assigned to surface fractals of the aggregates. Primary particles can be clearly identified as an upturn in SAXS intensity at $q \sim 0.3$ nm^{-1} via a Porod plot (see lowest pattern in Figure 9). Thus, SAXS patterns obtained for the original carbon black dispersion in n-dodecane can be interpreted in terms of scattering from primary particles (level 3), aggregates of these primary particles (level 2), and mass fractals of the aggregates (level 1) (see Table 1).

Structural characteristics of the carbon black can be determined by fitting the unified model to the scattering patterns (eq 5). A multilevel unified fit presented in a previous study[81] has been employed for the SAXS analysis in this work. The SAXS pattern for the initial dispersion of carbon black in n-dodecane is reasonably well described by this model (see Figures 8 and 9, the lowest patterns). The mean primary particle size, $2R_{g,3}$, is 13.8 nm (Table 1, level 3), which is comparable to data

DOI: 10.1021/acs.macromol.5b00517
Macromolecules 2015, 48, 3691−3704

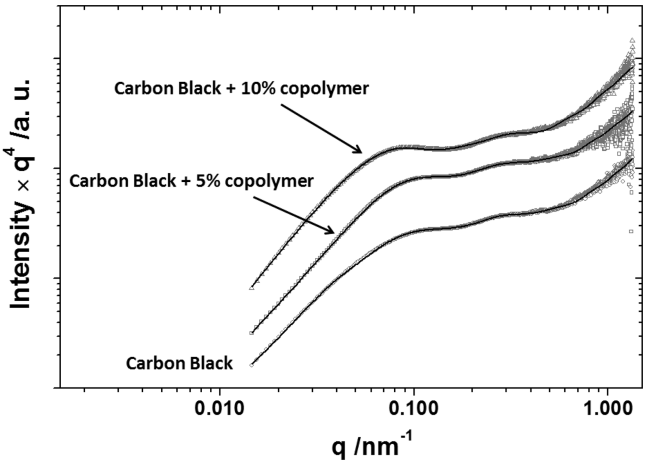

Figure 9. Porod plots of representative SAXS patterns recorded for 1.0% w/w carbon black dispersions in *n*-dodecane alone (circles) and in *n*-dodecane at two star diblock copolymer concentrations (5.0% w/w based on carbon black, squares; 10.0% w/w based on carbon black, triangles). Solid lines indicate multilevel unified fits to the experimental data.

reported in other studies.[78,81,85] The aggregate size, $2R_{g,2}$ = 96 nm (Table 1, level 2) is within the size range observed previously.[78] The power law exponent for these aggregates, P_2 = 4.0 (Table 1) (rather than the value of 3.8 estimated directly from the SAXS pattern, Figure 8), indicates a smooth electron density distribution at the aggregate surface, suggesting that the primary particles that make up these aggregates have a relatively smooth interface. It is usually found that the power law exponent for the aggregates ranges from 3.4 to 4.0,[78,81,82,84,89] indicating that the electron density distribution at the primary particle surface can vary according to the synthesis method and processing conditions. The validity parameter calculated for level 2 is close to the upper limit (Table 1), which is likely to be related to the relatively broad size distribution of the aggregates. The power law exponent of the mass fractals formed by the aggregates (Table 1, level 1) corresponds to a fractal dimension D_m (or P_1) of 2.6. A similar fractal dimension was observed for a diesel soot dispersed in acetone.[85] Thus, the structural morphology of the carbon black particles dispersed in *n*-dodecane can be described as relatively compact mass fractals (Figure 10a).

It was also found that incorporating an appropriate structure factor into the model produced a better fit to the region of the SAXS pattern corresponding to the primary particles (level 3). Further analysis revealed a weak correlation between the primary particles

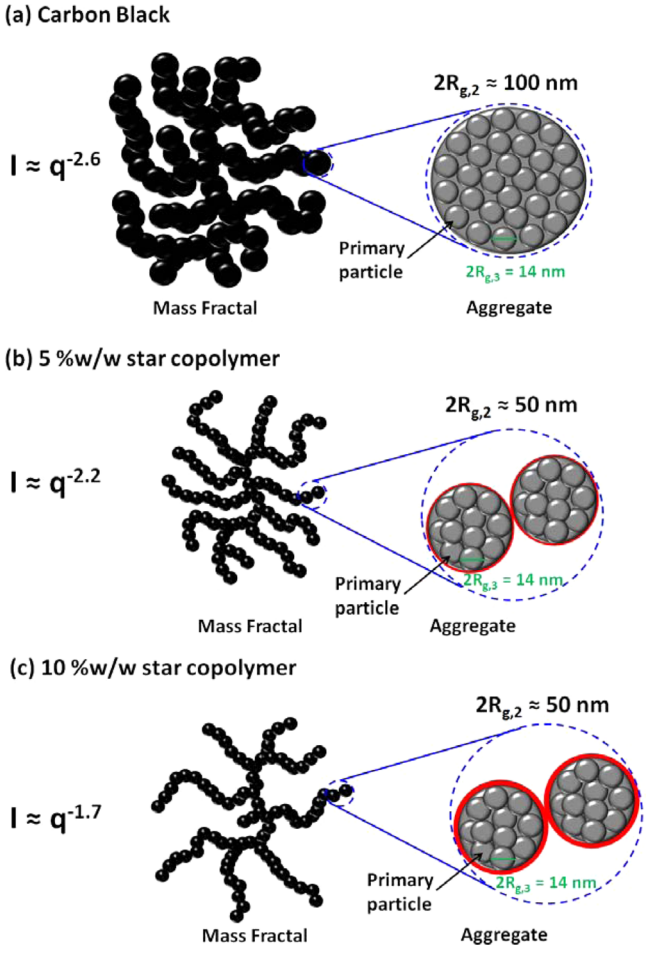

Figure 10. Structural morphologies and associated power law exponents for carbon black dispersions: (a) in *n*-dodecane alone; (b) in *n*-dodecane plus 5.0% w/w star diblock copolymer; (c) in *n*-dodecane plus 10.0% w/w star diblock copolymer. The red shell surrounding the aggregates depicts the likely location of the copolymer.

Table 1. Calculated Parameters for Three Hierarchical Structures (Levels) Derived from Multilevel Unified Fits to the Experimental SAXS Patterns Recorded for 1.0% w/w Carbon Black Dispersions; the Relevant Power Law Exponent (P_1, P_2, or P_3), the Size of the Structural Element ($2R_{g,2}$ or $2R_{g,3}$), the Validity Parameter (f_2 and f_3), the Correlation Distance ($R_{c,3}$) and the Degree of Correlation (η_3)[a]

	level 1 (agglomerates)	level 2 (aggregates)			level 3 (primary particles)				
star diblock copolymer added (copolymer mass based on mass of carbon black)	P_1	$2R_{g,2}$ (nm)	P_2	f_2	$2R_{g,3}$ (nm)	P_3	f_3	$R_{c,3}$	η_3
carbon black alone	2.6	96	4.0	2.2	13.8	1.9	−0.5	23	2.0
1.0% w/w	2.5	92	4.0	2.4	13.4	1.5	−0.6	23	2.1
2.0% w/w	2.6	86	4.0	3.5	13.8	1.9	−0.6	23	2.2
3.0% w/w	2.3	42	4.0	0.5	14.4	1.8	−0.7	26	2.2
4.0% w/w	2.2	46	4.0	0.8	14.8	2.0	−0.5	24	1.3
5.0% w/w	2.2	50	4.1	0.9	13.6	2.1	−0.4	23	1.8
7.0% w/w	2.2	56	4.1	0.6	14.0	1.8	−0.5	23	1.4
8.0% w/w	2.2	56	4.2	0.7	14.8	2.2	−0.4	23	1.0
9.0% w/w	1.9	62	4.3	0.9	14.0	2.0	−0.5	23	1.6
10.0% w/w	1.7	56	4.3	2.2	14.2	2.1	−0.1	20	1.8

[a]Errors in the fitted parameters shown in this table are within a unit of the last digit of the values given.

DOI: 10.1021/acs.macromol.5b00517
Macromolecules 2015, 48, 3691−3704

($\eta_3 < 3$, see Table 1). The power law exponent calculated for the primary particles, P_3, is also given in Table 1. This parameter is based on the scattering at high q. However, it is difficult to interpret such exponents as this region of the scattering pattern is also influenced by excess scattering from a smaller hierarchical carbon structure (subunits of ~1.5−2.0 nm) and also by internal inhomogeneities of carbon particles comprising crystalline and amorphous phases.[79,81,89] This is also reflected in the validity parameter for level 3, which is close to the lower limit (Table 1).

SAXS patterns recorded for the carbon black dispersion in *n*-dodecane in the presence of varying concentrations of the star diblock copolymer differ significantly compared to that observed for poorly dispersed carbon black particles alone in this solvent (Figures 8 and 9). On increasing the copolymer concentration, the gradient of the scattering intensity associated with the mass fractal dimension increases from −2.3 to −1.8, while that associated with the aggregate surface structure is reduced from −3.8 to −4.1 (Figure 8). Further structural information is obtained from detailed SAXS analysis. The multilevel unified model described by eq 5 produced reasonable fits to scattering patterns of the carbon black dispersions containing copolymer (Figures 8 and 9). Inspecting Table 1, the primary particle size remains approximately 14 nm (as found for the carbon black particles alone), with insignificant deviations in the other parameters associated with this structural level. These data suggest that addition of this copolymer to the carbon black essentially does not affect structural morphology associated with the primary particles. In contrast, pronounced changes are revealed in the other two structural levels on increasing the copolymer concentration. The mean aggregate size is reduced to 40−60 nm (Table 1 and Figure 11), which is comparable to the size of the aggregates observed for carbon black dispersions in toluene after being subjected to prolonged ultrasonic treatment.[81] The SAXS analysis shows that on addition of copolymer to the carbon black dispersion the validity parameter for level 2 increases initially at low copolymer concentrations but then decreases to values corresponding to the medium of the validity interval (Table 1) at higher copolymer concentrations. In the latter regime, the carbon black aggregate size is reduced by almost a factor of 2 compared to the original size. Therefore, the observed behavior of f_2 may be associated with broadening of the aggregate size distribution due to partial breakup of the aggregates at low copolymer concentrations, thus producing two populations comprising large and small aggregates (Table 1; see 1.0% w/w copolymer and 2.0% w/w copolymer entries). Complete breakup of the larger aggregates occurs at higher copolymer concentration, producing a single population of relatively small aggregates. This narrows the width of the size distribution; hence, the corresponding f_2 value is reasonably small.

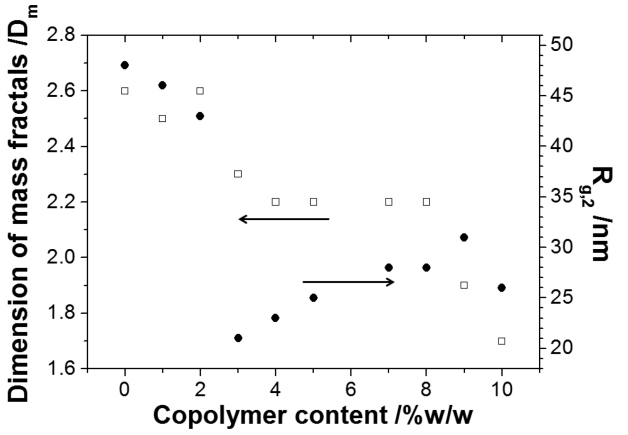

Figure 11. Change in mass fractal dimension, D_m ($D_m = P_1$, Table 1) (open squares), and radius of gyration of the carbon black aggregates, R_{g2} (filled circles), with increasing star diblock copolymer concentration for 1.0% w/w carbon black dispersions in *n*-dodecane.

The characteristic mass fractal dimension is gradually reduced from 2.6 to 1.7 (Table 1 and Figure 11). There is also a discernible increase in the power law exponent for the aggregates from 4.0 to 4.3 (P_2, Table 1). This observation is consistent with copolymer adsorption (see Figures 10b,c). In this case a copolymer shell of relatively low electron density covering electron-dense carbon black aggregates produces a diffuse interface between the aggregates and the surrounding environment, causing a negative deviation of the scattering intensity gradient from Porod's law, for which the gradient is equal to −4.0. Ruland's sigmoidal gradient model can be used in order to estimate the diffuse interface thickness associated with a negative deviation from Porod's law:[93,94]

$$I(q) = \frac{K}{q^4}\exp(\sigma^2 q^2) \tag{8}$$

where σ is the standard deviation of the Gaussian smoothing function related to the width of the transition zone, where K is a constant.[93] The interface thickness, t, can be calculated using $t = (2\pi)^{1/2}\sigma$.[94] SAXS analysis suggests that the most sensitive part of the scattering patterns related to the negative deviation of level 2 (Table 1, $P_2 > 4$) is in the q range from 0.1 to 0.2 nm^{-1} (Figure 9). Fitting Ruland's model to a power law function with an exponent of −4.3 within this q range indicates a negative deviation corresponding to an interface thickness of approximately 7.5 nm. The radius of gyration (R_g) of the star diblock copolymer can be estimated mathematically. The projected contour length for both polystyrene and 1,2-polyisoprene repeat units is 0.255 nm (i.e., two C−C bonds in an *all-trans* conformation), the total contour length of one arm of the star diblock copolymer (M_n = 384K, ~8 arms per star) = 666 × 0.255 nm = 170 nm. A mean Kuhn length of 1.72 nm (based on the known literature value for polyisoprene[95]) indicates an unperturbed radius of gyration, $R_g = (170 \times 1.72/6)^{0.5}$, or ~7 nm. Thus, the above adsorbed copolymer layer thickness of 7.5 nm suggests some degree of flattening of the star diblock copolymer when adsorbed onto the carbon black particles.

The observed changes in structural morphology with increasing copolymer concentration can be combined in the following model (see Figure 10). Adding ≥3.0% w/w star diblock copolymer breaks up the carbon black aggregates into smaller aggregates (see Figures 10b,c and 11). Simultaneously, the mass fractal dimension, D_m, is reduced from 2.6 to 1.7 (see Figure 11), suggesting the transformation of initially compact carbon black aggregates (see Figure 10a) into relatively loose aggregates (see Figure 10c). Moreover, a thicker adsorbed layer of copolymer is clearly formed on the latter aggregates when employing higher copolymer concentrations (Figures 10b,c).

■ CONCLUSIONS

In summary, this study demonstrates the value of utilizing multiple complementary characterization techniques that offer structural information over a range of length scales. Optical microscopy, TEM, and analytical centrifugation studies indicate

DOI: 10.1021/acs.macromol.5b00517
Macromolecules 2015, 48, 3691−3704

that the star diblock copolymer acts as a flocculant for carbon black in *n*-dodecane at relatively low copolymer concentrations, since bridging of the copolymer chains between multiple carbon black particles leads to the formation of aggregates and larger agglomerates. However, above a certain critical concentration (corresponding to a fractional surface coverage of 0.45 to 0.60), bridging is no longer favored; the star diblock copolymer acts as a steric stabilizer for the carbon black particles under these conditions. In this latter regime, analytical centrifugation requires knowledge of the effective density of the sterically stabilized carbon black particles, but fortunately this parameter can be calculated via Stokes' law (although not for all experimental conditions studied herein). The critical copolymer concentration required for steric stabilization was found to be somewhat solvent dependent but surprisingly independent of temperature.

SAXS studies enable three hierarchical structures to be identified for the carbon black used in this study. Scattering patterns obtained in *n*-dodecane can be interpreted in terms of scattering from primary particles, aggregates of these primary particles, and mass fractals of such aggregates. Furthermore, addition of the star diblock copolymer does not affect the primary structural morphology associated with the carbon black particles. However, pronounced changes are revealed in the other two structural levels on increasing the copolymer concentration. The mean aggregate size is reduced along with the characteristic mass fractal dimension. There is also an increase in the power law exponent for the aggregates from 4.0 to 4.3. This is consistent with a shell of relatively low electron density covering electron-dense carbon black aggregates, which hence offers direct evidence for copolymer adsorption. The observed changes in structural morphology with increasing copolymer concentration indicate that adding at least 3.0% w/w star diblock copolymer breaks up the relatively large, initially compact carbon black aggregates into smaller, looser aggregates. Furthermore, SAXS provides direct evidence for copolymer adsorption on the carbon black and allows an estimate of the adsorbed layer thickness.

■ ASSOCIATED CONTENT

Supporting Information

THF GPC and ^{1}H NMR ($CDCl_3$, 20 °C) analyses of the star diblock copolymer, digital images and schematic cartoon depicting gel network formation by the star diblock copolymer at high concentration, TEM image of Regal 250R carbon black, core-line X-ray photoelectron spectra for carbon black, adsorption isotherms and linear plots for star diblock copolymer adsorption onto carbon black from *n*-heptane, *n*-dodecane, and PAO2 base oil at 20 °C, adsorption isotherms for star diblock copolymer adsorption onto carbon black from *n*-dodecane at 20 °C (comparison of UV and TGA techniques), dynamic light scattering studies of a dilute star diblock copolymer solution in *n*-dodecane at 20 °C, tabulated Ostwald viscometry data for *n*-dodecane and d_{26}-dodecane at 20 °C, calculation of effective density for star copolymer-adsorbed carbon black particles using Stokes' law. The Supporting Information is available free of charge on the ACS Publications website at DOI: 10.1021/acs.macromol.5b00517.

■ AUTHOR INFORMATION

Corresponding Authors

*Tel 01142 229342; e-mail s.p.armes@shef.ac.uk (S.P.A.).
*Tel 01142 229418; e-mail o.mykhaylyk@shef.ac.uk (O.O.M.).

Notes

The authors declare no competing financial interest.

■ ACKNOWLEDGMENTS

BP Formulated Products Technology is thanked for funding a PhD studentship for D.J.G. Dr. D. Fomitchev of Cabot Corporation (Billerica, USA) is thanked for the kind donation of the Regal 250R carbon black particles. Dr Jan Ilavsky is thanked for providing detailed information about the unified fit protocol incorporated within SAS Irena macros for Igor Pro. The authors also acknowledge Diamond Light Source for synchrotron beam time and thank the I22 station personnel for their assistance with the SAXS experiments.

■ REFERENCES

(1) Ruehrwein, R. A.; Ward, D. W. Mechanism of clay aggregation by polyelectrolytes. *Soil Sci.* **1952**, *73*, 485−492.
(2) Biggs, S.; Habgood, M.; Jameson, G. J.; Yan, Y.-d. Aggregate structures formed via a bridging flocculation mechanism. *Chem. Eng. J.* **2000**, *80*, 13−22.
(3) Yan, Y.-d.; Burns, J. L.; Jameson, G. J.; Biggs, S. The structure and strength of depletion force induced particle aggregates. *Chem. Eng. J.* **2000**, *80*, 23−30.
(4) Glover, S. M.; Yan, Y.-d.; Jameson, G. J.; Biggs, S. Bridging flocculation studied by light scattering and settling. *Chem. Eng. J.* **2000**, *80*, 3−12.
(5) Gregory, J. Monitoring particle aggregation processes. *Adv. Colloid Interface Sci.* **2009**, *147−148*, 109−123.
(6) Heller, W.; Pugh, T. L. Steric" stabilization of colloidal solutions by adsorption of flexible macromolecules. *J. Polym. Sci.* **1960**, *47*, 203−217.
(7) Hiemenz, P. C.; Vold, R. D. Rates of flocculation and deflocculation in dispersions of carbon black in hydrocarbons. *J. Colloid Sci.* **1965**, *20*, 635−649.
(8) Napper, D. H. *Polymeric Stabilization of Colloidal Dispersions*; Academic Press: London, 1983; Vol. 7, pp 1−15.
(9) Vincent, B.; Edwards, J.; Emmett, S.; Jones, A. Depletion flocculation in dispersions of sterically-stabilised particles ("soft spheres"). *Colloids Surf.* **1986**, *18*, 261−281.
(10) Feigin, R. I.; Napper, D. H. Depletion stabilization and depletion flocculation. *J. Colloid Interface Sci.* **1980**, *75*, 525−541.
(11) Napper, D. H. Steric stabilization. *J. Colloid Interface Sci.* **1977**, *58*, 390−407.
(12) Jenkins, P.; Snowden, M. Depletion flocculation in colloidal dispersions. *Adv. Colloid Interface Sci.* **1996**, *68*, 57−96.
(13) Armes, S. P.; Aldissi, M. Preparation and characterization of colloidal dispersions of polypyrrole using poly(2-vinyl pyridine)-based steric stabilizers. *Polymer* **1990**, *31*, 569−574.
(14) Tadros, T. F. Steric stabilisation and flocculation by polymers. *Polym. J.* **1991**, *23*, 683−696.
(15) Whipple, W. L.; Maltesh, C. Adsorption of cationic flocculants to paper slurries. *J. Colloid Interface Sci.* **2002**, *256*, 33−40.
(16) Zeng, D.; Wu, J.; Kennedy, J. F. Application of a chitosan flocculant to water treatment. *Carbohydr. Polym.* **2008**, *71*, 135−139.
(17) Singh, R.; Nayak, B.; Biswal, D.; Tripathy, T.; Banik, K. Biobased polymeric flocculants for industrial effluent treatment. *Mater. Res. Innovations* **2003**, *7*, 331−340.
(18) Weissenborn, P. K.; Warren, L. J.; Dunn, J. G. Optimisation of selective flocculation of ultrafine iron ore. *Int. J. Miner. Process.* **1994**, *42*, 191−213.
(19) Bolto, B. A. Soluble polymers in water purification. *Prog. Polym. Sci.* **1995**, *20*, 987−1041.
(20) Pelton, R. H. A model for flocculation in turbulent flow. *Colloids Surf.* **1981**, *2*, 259−275.
(21) Alonzo, J.; Hinestrosa, J. P.; Mays, J. W.; Kilbey, S. M. Kinetics of preferential adsorption of amphiphilic star block copolymers that tether by their corona blocks at the solid/fluid interface. *Macromolecules* **2014**, *47*, 4048−4055.

DOI: 10.1021/acs.macromol.5b00517
Macromolecules 2015, 48, 3691−3704

(22) Stoll, S.; Buffle, J. Computer simulation of bridging flocculation processes: the role of colloid to polymer concentration ratio on aggregation kinetics. *J. Colloid Interface Sci.* **1996**, *180*, 548−563.
(23) Healy, T. W.; La Mer, V. K. The energetics of flocculation and redispersion by polymers. *J. Colloid Sci.* **1964**, *19*, 323−332.
(24) Lu, C.; Pelton, R. PEO flocculation of polystyrene-core poly(vinylphenol)-shell latex: an example of ideal bridging. *Langmuir* **2001**, *17*, 7770−7776.
(25) McFarlane, N. L.; Wagner, N. J.; Kaler, E. W.; Lynch, M. L. Poly(ethylene oxide) (PEO) and poly(vinyl pyrolidone) (PVP) induce different changes in the colloid stability of nanoparticles. *Langmuir* **2010**, *26*, 13823−13830.
(26) Santore, M. M.; Russel, W. B.; Prud'homme, R. K. Experimental and theoretical study of phase transitions induced in colloidal dispersions by associative polymers. *Faraday Discuss. Chem. Soc.* **1990**, *90*, 323−333.
(27) Hoogeveen, N. G.; Cohen Stuart, M. A.; Fleer, G. J. Can charged (block co)polymers act as stabilisers and flocculants of oxides? *Colloids Surf., A* **1996**, *117*, 77−88.
(28) Snowden, M. J.; Clegg, S. M.; Williams, P. A.; Robb, I. D. Flocculation of silica particles by adsorbing and non-adsorbing polymers. *J. Chem. Soc., Faraday Trans.* **1991**, *87*, 2201−2207.
(29) Solberg, D.; Wågberg, L. Adsorption and flocculation behavior of cationic polyacrylamide and colloidal silica. *Colloids Surf., A* **2003**, *219*, 161−172.
(30) Overbeek, J. T. G. Colloid stability in aqueous and non-aqueous media. Introductory paper. *Discuss. Faraday Soc.* **1966**, *42*, 7−13.
(31) Bhattacharjee, S.; Paria, M. K.; Maiti, H. S. Polyvinyl butyral as a dispersant for barium titanate in a non-aqueous suspension. *J. Mater. Sci.* **1993**, *28*, 6490−6495.
(32) Ma, S.-H.; Matrick, H.; Shor, A. C.; Spinelli, H. J. Aqueous pigmented inks for ink jet printers. US Patent 5,085,698, 1992.
(33) Croll, S. DLVO theory applied to TiO_2 pigments and other materials in latex paints. *Prog. Org. Coat.* **2002**, *44*, 131−146.
(34) Reuter, E.; Silber, S.; Psiorz, C. The use of new block copolymeric dispersing agents for waterborne paints — theoretical and practical aspects. *Prog. Org. Coat.* **1999**, *37*, 161−167.
(35) Shar, J. A.; Cosgrove, T.; Obey, T. M.; Warne, M. R.; Wedlock, D. J. Adsorption studies of diblock copolymers at the cyclohexane/carbon black interface. *Langmuir* **1999**, *15*, 7688−7694.
(36) Cawdery, N.; Obey, T. M.; Vincent, B. Colloidal dispersions of electrically conducting polypyrrole particles in various media. *J. Chem. Soc., Chem. Commun.* **1988**, 1189−1190.
(37) Armes, S. P.; Vincent, B. Dispersions of electrically conducting polypyrrole particles in aqueous media. *J. Chem. Soc., Chem. Commun.* **1987**, 288−290.
(38) Armes, S. P.; Aldissi, M. Novel colloidal dispersons of polyaniline. *J. Chem. Soc., Chem. Commun.* **1989**, 88−89.
(39) Simmons, M. R.; Chaloner, P. A.; Armes, S. P.; Greaves, S. J.; Watts, J. F. Synthesis and characterization of colloidal polypyrrole particles using reactive polymeric stabilizers. *Langmuir* **1998**, *14*, 611−618.
(40) Armes, S. P.; Aldissi, M. Preparation and characterization of colloidal dispersions of polypyrrole using poly(2-vinyl pyridine)-based steric stabilizers. *Polymer* **1990**, *31*, 569−574.
(41) Kim, J. H.; Chainey, M.; El-Aasser, M. S.; Vanderhoff, J. W. Preparation of highly sulfonated polystyrene model colloids. *J. Polym. Sci., Part A: Polym. Chem.* **1989**, *27*, 3187−3199.
(42) Lok, K. P.; Ober, C. K. Particle size control in dispersion polymerization of polystyrene. *Can. J. Chem.* **1985**, *63*, 209−216.
(43) O'Neill, M. L.; Yates, M. Z.; Harrison, K. L.; Johnston, K. P.; Canelas, D. A.; Betts, D. E.; DeSimone, J. M.; Wilkinson, S. P. Emulsion stabilization and flocculation in CO_2. 1. Turbidimetry and tensiometry. *Macromolecules* **1997**, *30*, 5050−5059.
(44) Richez, A. P.; Yow, H. N.; Biggs, S.; Cayre, O. J. Dispersion polymerization in non-polar solvent: evolution toward emerging applications. *Prog. Polym. Sci.* **2013**, *38*, 897−931.
(45) Au, K. M.; Armes, S. P. Heterocoagulation as a facile route to prepare stable serum albumin-nanoparticle conjugates for biomedical applications: synthetic protocols and mechanistic insights. *ACS Nano* **2012**, *6*, 8261−8279.
(46) Simmons, M. R.; Patrickios, C. S. Synthesis and aqueous solution characterization of catalytically active block copolymers containing imidazole. *Macromolecules* **1998**, *31*, 9075−9077.
(47) Baines, F. L.; Billingham, N. C.; Armes, S. P. Synthesis and solution properties of water-soluble hydrophilic−hydrophobic block copolymers. *Macromolecules* **1996**, *29*, 3416−3420.
(48) Wilhelm, M.; Zhao, C. L.; Wang, Y.; Xu, R.; Winnik, M. A.; Mura, J. L.; Riess, G.; Croucher, M. D. Poly(styrene-ethylene oxide) block copolymer micelle formation in water: a fluorescence probe study. *Macromolecules* **1991**, *24*, 1033−1040.
(49) Dawkins, J. V.; Maghami, G. G.; Shakir, S. A.; Higgins, J. S. Non-aqueous polymer dispersions: radical dispersion polymerization in the presence of the diblock copolymer poly(styrene-b-[ethylene-co-propylene]). *Colloid Polym. Sci.* **1986**, *264*, 616−618.
(50) Vincent, B.; Waterson, J. Colloidal dispersions of electrically-conducting, spherical polyaniline particles. *J. Chem. Soc., Chem. Commun.* **1990**, 683−684.
(51) Hadjichristidis, N.; Pispas, S.; Floudas, G. *Block Copolymers: Synthetic Strategies, Physical Properties, and Applications*; John Wiley & Sons: New York, 2003; pp 47−65.
(52) Hadjichristidis, N.; Pitsikalis, M.; Pispas, S.; Iatrou, H. Polymers with complex architecture by living anionic polymerization. *Chem. Rev.* **2001**, *101*, 3747−3792.
(53) Burguiere, C.; Dourges, M. A.; Charleux, B.; Vairon, J. P. Synthesis and characterization of omega-unsaturated poly(styrene-b-n-butyl methacrylate) block copolymers using TEMPO-mediated controlled radical polymerization. *Macromolecules* **1999**, *32*, 3883−3890.
(54) Quaglia, F.; Ostacolo, L.; De Rosa, G.; La Rotonda, M. I.; Ammendola, M.; Nese, G.; Maglio, G.; Palumbo, R.; Vauthier, C. Nanoscopic core-shell drug carriers made of amphiphilic triblock and star-diblock copolymers. *Int. J. Pharm.* **2006**, *324*, 56−66.
(55) Li, Y.; Narain, R.; Ma, Y.; Lewis, A. L.; Armes, S. P. Biomimetic thermo-responsive star diblock gelators. *Chem. Commun.* **2004**, 2746−2747.
(56) Xia, J.; Zhang, X.; Matyjaszewski, K. Synthesis of star-shaped polystyrene by atom transfer radical polymerization using an "arm first" approach. *Macromolecules* **1999**, *32*, 4482−4484.
(57) Gao, H.; Matyjaszewski, K. Synthesis of star polymers by a combination of ATRP and the "click" coupling method. *Macromolecules* **2006**, *39*, 4960−4965.
(58) Haddleton, D. M.; Crossman, M. C. Synthesis of methacrylic multi-arm star copolymers by "arm-first" group transfer polymerisation. *Macromol. Chem. Phys.* **1997**, *198*, 871−881.
(59) Li, Y.; Tang, Y.; Narain, R.; Lewis, A. L.; Armes, S. P. Biomimetic stimulus-responsive star diblock gelators. *Langmuir* **2005**, *21*, 9946−9954.
(60) Eckert, R. J. Hydrogenated star-shaped polymer. US Patent 4116917, 1978.
(61) Coessens, V.; Pintauer, T.; Matyjaszewski, K. Functional polymers by atom transfer radical polymerization. *Prog. Polym. Sci.* **2001**, *26*, 337−377.
(62) Chong, Y.; Le, T. P.; Moad, G.; Rizzardo, E.; Thang, S. H. A more versatile route to block copolymers and other polymers of complex architecture by living radical polymerization: the RAFT process. *Macromolecules* **1999**, *32*, 2071−2074.
(63) Ilavsky, J.; Jemian, P. R. Irena: tool suite for modeling and analysis of small-angle scattering. *J. Appl. Crystallogr.* **2009**, *42*, 347−353.
(64) Scares, B. G.; de Souza Gomes, A. Spectrophotometric determination of the styrene content of alpha-methylstyrene—styrene copolymers. *Polym. Bull.* **1988**, *20*, 543−548.
(65) Godward, J.; Heatley, F.; Price, C. 1 H Nuclear magnetic relaxation study of the phase structure of polystyrene-*block*-poly (ethylene/propylene) copolymer micelles. *J. Chem. Soc., Faraday Trans.* **1993**, *89*, 3471−3475.
(66) Clague, A. D. H.; Donnet, J. B.; Wang, T. K.; Peng, J. C. M. A comparison of diesel engine soot with carbon black. *Carbon* **1999**, *37*, 1553−1565.

DOI: 10.1021/acs.macromol.5b00517
Macromolecules 2015, 48, 3691−3704

(67) Won, Y.-Y.; Meeker, S. P.; Trappe, V.; Weitz, D. A.; Diggs, N. Z.; Emert, J. I. Effect of temperature on carbon-black agglomeration in hydrocarbon liquid with adsorbed dispersant. *Langmuir* **2004**, *21*, 924−932.
(68) Pugh, R. J.; Matsunaga, T.; Fowkes, F. M. The dispersibility and stability of carbon black in media of low dielectric constant. 1. Electrostatic and steric contributions to colloidal stability. *Colloids Surf.* **1983**, *7*, 183−207.
(69) Pugh, R. J.; Fowkes, F. M. The dispersibility and stability of carbon black in media of low dielectric constant. 2. Sedimentation volume of concentrated dispersions, adsorption and surface calorimetry studies. *Colloids Surf.* **1984**, *9*, 33−46.
(70) Growney, D. J.; Mykhaylyk, O. O.; Armes, S. P. Micellization and adsorption behavior of a near-monodisperse polystyrene-based diblock copolymer in nonpolar media. *Langmuir* **2014**, *30*, 6047−6056.
(71) Cohen Stuart, M. A.; Cosgrove, T.; Vincent, B. Experimental aspects of polymer adsorption at solid/solution interfaces. *Adv. Colloid Interface Sci.* **1985**, *24*, 143−239.
(72) Ho, Y.-S. Isotherms for the sorption of lead onto peat: comparison of linear and non-linear methods. *Pol. J. Environ. Stud.* **2006**, *15*, 81−86.
(73) Fleer, G. J.; Cohen Stuart, M. A.; Scheutjens, J. M. H. M.; Cosgrove, T.; Vincent, B. *Polymers at Interfaces*; Chapman and Hall: London, 1993; pp 66−76.
(74) Huang, J.-C. Carbon black filled conducting polymers and polymer blends. *Adv. Polym. Technol.* **2002**, *21*, 299−313.
(75) Detloff, T.; Sobisch, T.; Lerche, D. Particle size distribution by space or time dependent extinction profiles obtained by analytical centrifugation. *Part. Part. Syst. Charact.* **2006**, *23*, 184−187.
(76) Lutskii, A. Molecular constants and the viscosity of liquids. *Zh. Fiz. Khim.* **1955**, *29*, 1162−1172.
(77) Viswanath, D. S.; Ghosh, T. K.; Prasad, D. H. L.; Dutt, N. V. K.; Rani, K. Y. *Viscosity of Liquids: Theory, Estimation, Experiment, and Data*; Springer: Berlin, 2007; p 307.
(78) Braun, A.; Huggins, F. E.; Seifert, S.; Ilavsky, J.; Shah, N.; Kelly, K. E.; Sarofim, A.; Huffman, G. P. Size-range analysis of diesel soot with ultra-small angle X-ray scattering. *Combust. Flame* **2004**, *137*, 63−72.
(79) di Stasio, S.; Mitchell, J. B. A.; LeGarrec, J. L.; Biennier, L.; Wulff, M. Synchrotron SAXS (in situ) identification of three different size modes for soot nanoparticles in a diffusion flame. *Carbon* **2006**, *44*, 1267−1279.
(80) Hessler, J. P.; Seifert, S.; Winans, R. E.; Fletcher, T. H. Small-angle X-ray studies of soot inception and growth. *Faraday Discuss.* **2001**, *119*, 395−407.
(81) Koga, T.; Hashimoto, T.; Takenaka, M.; Aizawa, K.; Amino, N.; Nakamura, M.; Yamaguchi, D.; Koizumi, S. New insight into hierarchical structures of carbon black dispersed in polymer matrices: A combined small-angle scattering study. *Macromolecules* **2008**, *41*, 453−464.
(82) Sorensen, C. M.; Oh, C.; Schmidt, P. W.; Rieker, T. P. Scaling description of the structure factor of fractal soot composites. *Phys. Rev. E* **1998**, *58*, 4666−4672.
(83) Koga, T.; Takenaka, M.; Aizawa, K.; Nakamura, M.; Hashimoto, T. Structure factors of dispersible units of carbon black filler in rubbers. *Langmuir* **2005**, *21*, 11409−11413.
(84) Rieker, T. P.; Hindermann-Bischoff, M.; Ehrburger-Dolle, F. Small-angle X-ray scattering study of the morphology of carbon black mass fractal aggregates in polymeric composites. *Langmuir* **2000**, *16*, 5588−5592.
(85) Braun, A.; Ilavsky, J.; Seifert, S.; Jemian, P. R. Deformation of diesel soot aggregates as a function of pellet pressure: A study with ultra-small-angle x-ray scattering. *J. Appl. Phys.* **2005**, *98*, 073513−1−073513−5.
(86) Beaucage, G. Approximations leading to a unified exponential power-law approach to small-angle scattering. *J. Appl. Crystallogr.* **1995**, *28*, 717−728.
(87) Beaucage, G. Small-angle scattering from polymeric mass fractals of arbitrary mass-fractal dimension. *J. Appl. Crystallogr.* **1996**, *29*, 134−146.
(88) Beaucage, G.; Schaefer, D. W. Structural studies of complex-systems using small-angle scattering - A unified guinier power-law approach. *J. Non-Cryst. Solids* **1994**, *172*, 797−805.
(89) Braun, A.; Shah, N.; Huggins, F. E.; Kelly, K. E.; Sarofim, A.; Jacobsen, C.; Wirick, S.; Francis, H.; Ilavsky, J.; Thomas, G. E.; Huffman, G. P. X-ray scattering and spectroscopy studies on diesel soot from oxygenated fuel under various engine load conditions. *Carbon* **2005**, *43*, 2588−2599.
(90) Hammouda, B. Analysis of the Beaucage model. *J. Appl. Crystallogr.* **2010**, *43*, 1474−1478.
(91) Beaucage, G.; Kammler, H. K.; Pratsinis, S. E. Particle size distributions from small-angle scattering using global scattering functions. *J. Appl. Crystallogr.* **2004**, *37*, 523−535.
(92) Beaucage, G.; Ulibarri, T. A.; Black, E. P.; Schaefer, D. W. Multiple size scale structures in silica-siloxane composites studied by small-angle scattering. In *Hybrid Organic-Inorganic Composites*; American Chemical Society: Washington, DC, 1995; Vol. *585*, pp 97−111.
(93) Ruland, W. Small-angle scattering of two-phase systems: determination and significance of systematic deviations from Porod's law. *J. Appl. Crystallogr.* **1971**, *4*, 70−73.
(94) Roe, R. J. *Methods of X-ray and Neutron Scattering in Polymer Science*; Oxford University Press: New York, 2000; pp 185−188.
(95) Fetters, L. J.; Lohse, D. J.; Richter, D.; Witten, T. A.; Zirkel, A. Connection between polymer molecular weight, density, chain dimensions, and melt viscoelastic properties. *Macromolecules* **1994**, *27*, 4639−4647.

DOI: 10.1021/acs.macromol.5b00517
Macromolecules 2015, 48, 3691−3704